Imaging spin diffusion in germanium at room temperature

C. Zucchetti,[1] F. Bottegoni,[1] C. Vergnaud,[2] F. Ciccacci,[1] G. Isella,[1] L. Ghirardini,[1] M. Celebrano,[1] F. Rortais,[2] A. Ferrari,[2] A. Marty,[2] M. Finazzi,[1,*] and M. Jamet[2]

[1]*LNESS-Dipartimento di Fisica, Politecnico di Milano, 20133 Milano, Italy*

[2]*Spintec, Institut Nanosciences et Cryogénie, Université Grenoble Alpes, CEA, CNRS, F-38000 Grenoble, France*

(Received 24 March 2017; revised manuscript received 17 May 2017; published 5 July 2017)

We report on the nonlocal detection of optically oriented spins in lightly n-doped germanium at room temperature. Localized spin generation is achieved by scanning a circularly polarized laser beam ($\lambda = 1550$ nm) on an array of lithographically defined Pt microstructures. The in-plane oriented spin generated at the edges of such microstructures, placed at different distances from a spin-detection element, allows for a direct imaging of spin diffusion in the semiconductor, leading to a measured spin diffusion length of about 10 μm. Two different spin-detection blocks are employed, consisting of either a magnetic tunnel junction or a platinum stripe where the spin current is converted in an electrical signal by the inverse spin-Hall effect. The second solution represents the realization of a nonlocal spin-injection/detection scheme that is completely free from ferromagnetic functional blocks.

DOI: 10.1103/PhysRevB.96.014403

I. INTRODUCTION

The aim of spintronics is to exploit the spin degree of freedom to manipulate information, which, in conventional electronics, is instead associated only with the charge of carriers [1–3]. In this regard, germanium appears as a promising hosting material for spin transport and manipulation. The electron spin lifetime can reach several nanoseconds at room temperature [4], and the compatibility with mainstream silicon technology allows us to exploit the spin-related properties of low-dimensional SiGe heterostructures [5–7]. Moreover, selection rules for the absorption of circularly polarized light at the direct gap of Ge, which perfectly matches the 1550 nm telecom wavelength, enable spin injection by means of optical spin orientation [8]. Once optically excited at the Γ point, electrons are scattered to the L valleys of the Brillouin zone while still maintaining, at least partially, their spin polarization [6,9–11]. The long-lived L states can then be used for spin transport and detection [12–15].

Electrical spin injection and detection have been explored in Ge films or nanowires using either nonlocal measurements in lateral or vertical spin valves [16–19] or the Hanle effect in three-terminal devices [20–27]. The nonlocal lateral geometry is particularly interesting in spintronics since it allows, in principle, spin manipulation in the channel between the spin injector and detector. However, experimental measurements based on magnetic tunnel junctions (MTJs) have been limited in temperature to 225 K (Ref. [16]), and the only demonstration at room temperature was performed indirectly using a method combining spin pumping and the inverse spin Hall effect (ISHE) [28].

Here we implement a nonlocal spin-injection/detection scheme in germanium at room temperature, adding additional functionalities to the common architectures available for spintronic devices. By exploiting optical spin generation and a set of lithographically defined metal microstructures, we demonstrate lateral spin transport in a lightly n-doped bulk Ge sample. Nonlocal spin detection is achieved using either an MTJ or the ISHE in a Pt stripe. With this setup we directly show optical mapping of spin diffusion in Ge, and, by combining optical spin orientation and the ISHE in Pt, we build a nonlocal spin-injection/detection scheme without the use of any ferromagnetic metal. We find a spin diffusion length of about 10 μm at room temperature, making germanium an ideal platform for fundamental and applied research in spintronics.

II. SAMPLE PREPARATION AND EXPERIMENTAL SETUP

A Ge(001) substrate n-doped with As ($n = 1.7 \times 10^{16}$ cm^{-3}) was first cleaned in acetone and isopropyl alcohol in an ultrasonic bath for 5 min and then rinsed in deionized water before being loaded into a molecular beam epitaxy chamber. Successively, the native Ge oxide was thermally removed by annealing under ultrahigh vacuum to obtain a well-defined (2×1) surface reconstruction, as detected by reflection high-energy electron diffraction. For the MTJ device [see Fig. 1(a)], we first deposited an 8-nm-thick MgO layer at 310 °C, followed by 10 min of annealing at 650 °C and by room-temperature deposition of 15 nm of Pt. Eight 1×2 μm^2 Pt/MgO pads separated by 1 μm were then patterned by electron beam lithography and ion beam etching. Finally, an MTJ consisting of a Pt(5 nm)/Fe(15 nm)/MgO(3.5 nm) stack was grown at room temperature by electron beam evaporation and laterally defined by electron beam lithography. For the ISHE device [see Fig. 1(d)], starting from the same Ge surface, only a 15-nm-thick Pt layer was grown on Ge at room temperature, with no MgO capping to allow electrons photogenerated in the Ge substrate to diffuse into the Pt ISHE detector through the Schottky barrier at the Pt/Ge interface, as discussed in Refs. [29,30]. Eight Pt pads (identical to those fabricated on the MTJ device) and a 3×1 μm^2 Pt stripe for ISHE detection were then patterned by electron beam lithography and ion beam etching. Both MTJ and ISHE detectors were contacted by depositing an Au(250 nm)/Ti(10 nm) stack after passivating the surface with a 100-nm-thick SiO_2 layer. The magnetization of the MTJ layers and the position of the contacts on the Pt ISHE stripe are such that the measured signal in both detectors

*marco.finazzi@polimi.it

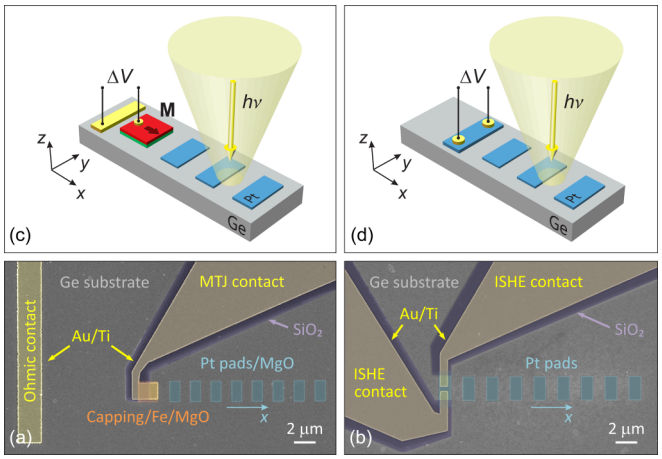

FIG. 1. Lateral devices for optical spin generation and nonlocal electrical spin detection. Scanning electron microscopy images (a), (b) and corresponding sketches (c) ,(d) of the MTJ and ISHE devices, respectively. For the MTJ device, the spin-induced electrical signal is measured between the top layer and an Ohmic contact made of Au(250 nm)/Ti(10 nm) directly grown on Ge, while the ISHE signal is measured across the Pt stripe.

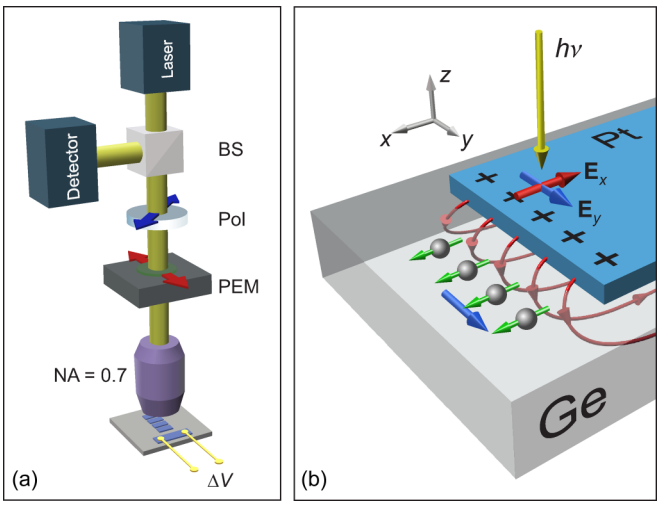

FIG. 2. (a) Optical apparatus: BS denotes beam splitter, PEM denotes photoelastic modulator, and Pol denotes polarizer. (b) Optical generation of in-plane spin-polarized electrons. When the light beam is focused at the edges of a Pt pad, the x component (red arrow) of the circularly polarized illuminating field induces antiphase oscillating charges that, in turn, generate a staticlike near field (red field lines). Such a quasistatic field has a strong z component that, combining with the $\pi/2$ dephased y component of the illuminating field (blue arrows), produces a circularly polarized electric field able to photoexcite in-plane spin-polarized electrons (green arrows). A complementary spin polarization is generated at the opposite edge.

is sensitive only to the in-plane spin polarization in the x direction of Figs. 1(c) and 1(d).

Optical spin orientation is performed by inserting the samples in a confocal scanning microscopy setup [Fig. 2(a)]. Illumination is provided by a continuous-wave laser diode working at a wavelength $\lambda = 1550\,\text{nm}$ ($h\nu = 0.8\,\text{eV}$), resonant with the direct band gap of Ge. The numerical aperture of the objective is 0.7, giving a full width at half-maximum beam size of approximately 1.5 μm. The light is circularly polarized using the combination of a polarizer rotated at 45° with respect to the axes of a photoelastic modulator. The circular polarization is modulated at 50 kHz, allowing for the synchronous detection of the electrical signal ΔV with a lock-in amplifier. Maps of the ΔV signal from the spin detectors as a function of the position of the circularly polarized light beam were obtained by raster-scanning the sample. Optical images were also simultaneously collected by recording the reflected light from the sample with a near-infrared InGaAs detector.

The generation of a spin-polarized electron population in the semiconductor occurs through the optical spin orientation process [8], which consists of the absorption of circularly polarized light that generates spin-polarized electron-hole pairs at the Γ point of the Brillouin zone. The spin polarization of photogenerated electrons in the conduction band is $P = (n_\uparrow - n_\downarrow)/(n_\uparrow + n_\downarrow)$, where $n_{\uparrow(\downarrow)}$ is the spin-up (-down) density referred to the quantization axis given by the direction of the light wave vector in the material. Photogenerated holes are rapidly depolarized due to their very short spin lifetime [22]. If the incident photon energy is tuned to the direct Ge band gap, an electron spin polarization $P = 50\%$ can be achieved [31]. Right after the photogeneration, spin-oriented electrons thermalize from the Γ to the L valleys within approximately 300 fs, maintaining most of their spin polarization [6,8,9].

At normal incidence on a uniform sample, only an out-of-plane spin polarization is generated, preventing any electrical spin detection in Ge with in-plane MTJ or ISHE detectors. The Pt pad pattern allows us to circumvent this limitation, as already demonstrated in Ref. [32]. The physics of the process, which has been rigorously analyzed also by means of numerical simulations [32], is schematized in Fig. 2(b): when the sample is illuminated with circularly polarized light focused at the edge of a Pt pad, the x component E_x of the field [red arrow in Fig. 2(b)] induces charges that generate in the Ge substrate a near-field with a large component in the z direction. The latter is in antiphase with respect to E_x because the illumination wavelength of 1550 nm is significantly shorter than those corresponding to the main plasmonic resonances of the Pt pad. The combination of the z component of the near-field with the $\pi/2$ phase-shifted y component E_y of the incoming light [blue arrows in Fig. 2(b)] results in an elliptic field polarization in the yz plane that can generate electrons with spin polarization along the x axis. Opposite spin polarizations are attained at opposite edges of the Pt pads. The resulting spin accumulation creates a pure spin current (with no associated charge transport) detected nonlocally by either the MTJ or the ISHE detector. The same [not shown in Fig. 2(b)] also applies at correspondence with the edges perpendicular to the y axis, where polarized photoelectrons are excited with spin oriented in the y direction. However, our spin MTJ- or ISHE-based detection schemes are not sensitive to this polarization axis, and no signal is measured when the beam is focused on such edges.[1] An interesting feature that makes local

[1]It is worth noticing that MTJ and ISHE detectors have been designed to avoid spurious electrical effects related to the electron diffusion. At variance from Ref. [32], where the ISHE detection was

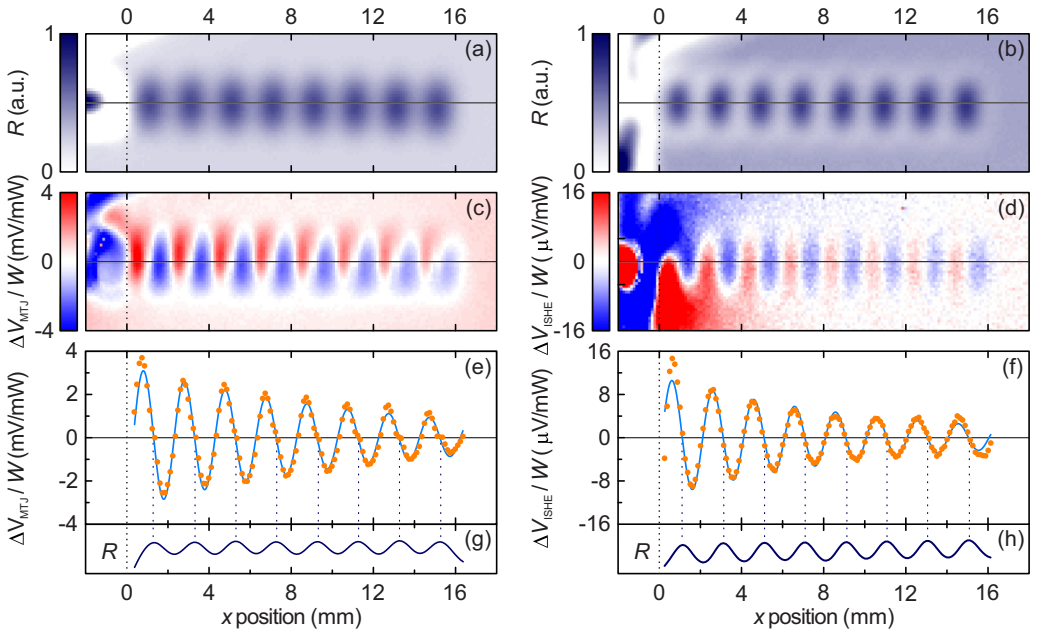

FIG. 3. (a), (b) Reflectivity (R) optical images recorded on the MTJ and ISHE devices, respectively. (c), (d) Corresponding simultaneously recorded MTJ and ISHE voltage signals. The incident power is 60 μW for the MTJ sensor and 900 μW for the ISHE detector. (e), (f) Voltage profiles along x across the centers of the Pt pads. In both cases, the detector is located at $x = 0$. The dots are the experimental data while the solid lines correspond to fits (see the text for the fitting function). The signals have been normalized to the laser power W. As illustrated by the dotted vertical line, corresponding to the maxima of the reflectivity R profiles in (g) and (h), the signal is zero at the center of each Pt pad and positive (negative) on the left (right) edge.

optical injection exploiting a patterned substrate competitive with other spin injection schemes consists in the fact that optical spin injection is completely free from reproducibility issues, since it does not depend on the quality of the interfaces defined by the Pt pads that modulate the light polarization inside the semiconducting substrate.

III. RESULTS AND DISCUSSION

The optical images of the nanostructures are shown in Figs. 3(a) (MTJ device) and 3(b) (ISHE device), while the room-temperature voltage signals are displayed in Fig. 3(c) for the MTJ (incident power $W = 60$ μW) and in Fig. 3(d) for the Pt ISHE detector (incident power $W = 900$ μW), respectively. In Figs. 3(e) and 3(f), the line profiles of the MTJ and ISHE voltage signals across the centers of the Pt pads are reported as a function of the distance to the detector. When the photon beam illuminates the Pt pad edges, an alternating signal is observed, indicating opposite spin polarization injected at opposite edges. The amplitude of the oscillation decays when the beam is moved away from the detector as a consequence of the finite spin diffusion length in Ge. The possibility of varying the distance separating the spin injector from the detector allows for the measurement of the *relative* variation of the spin signal. Therefore, the fitting procedure can be performed using the spin diffusion length as the only relevant free parameter. At variance, in nonlocal experiments where the distance between the injector and the detector is fixed, the absolute spin signal variation must be fitted by means of a suitable model, which typically requires the knowledge of several physical quantities related to the efficiency of spin injection and detection [16,17,23,33,34]. As shown in Figs. 3(e) and 3(f), the voltage ΔV normalized to the light power W can be accurately fitted using an exponentially decaying sinusoidal function: $\Delta V/W = Ae^{-x/l_{sf}} \sin(2\pi x/L)$, where $L = 2$ μm is the pattern periodicity, l_{sf} is the spin diffusion length, and $x = 0$ corresponds to the position of the detector.

By employing such a fitting expression, we implicitly assume a one-dimensional spin diffusion model, which is a rough approximation considering the three-dimensional geometry of our system. However, the very good agreement between the fitting curve and the experimental data suggests that the spin diffusion mostly takes place along x, which is probably due to the partial spin absorption by the Pt pads, which focus spin transport close to the Ge surface. We find $l_{sf} = 12 \pm 1$ μm for the MTJ device and $l_{sf} = 10 \pm 1$ μm for the ISHE device. The small difference between the diffusion lengths obtained for the two devices might be related to the presence, in the MTJ device, of the MgO layer, which partially prevents spin diffusion from the Ge substrate toward the Pt pads that act as spin sinks. Indeed, in a separate experiment an MgO layer was inserted between the ISHE Pt stripe and the substrate. In that case, a dramatic reduction of the ISHE detector efficiency was observed, confirming this picture.

performed with a continuous thin Pt film, we do not measure sizable signals related to a component of the spin-polarization parallel to the Pt pad edge with a bar-shaped ISHE detector. This indicates that the electromagnetic field modulation, operated by the Pt scatterers, mostly generates two complementary in-plane components of the spin polarization, perpendicular to the pad edges.

Assuming an electron diffusion coefficient in the Ge substrate equal to $D = 65\ \mathrm{cm^2\,s^{-1}}$, [35] in the MgO-capped device we find a spin lifetime $\tau_{sf} = 20 \pm 5$ ns, which is much larger than the theoretical estimation by Li *et al.* [4], later corrected by Yu and Wu up to $\tau_{sf} \approx 5.3$ ns [36]. However, in Ref. [4] the intervalley spin-flip scattering rate was obtained by evaluating two matrix elements ($D_{X1,s}$ and $D_{X4,s}$) with an empirical pseudopotential method and not from experimental data or rigorous symmetry arguments. Our results thus allow us to refine the parameters in the calculations by Li *et al.*, in particular by suggesting that the $D_{X1,s}$ and $D_{X4,s}$ coefficients are both overestimated by a factor of about 2.

As a final remark, we would like to stress that the comparison between the MTJ and the ISHE detection clearly demonstrates the validity of the latter as a viable means to sample local spin currents. The combination of optical spin orientation with in-plane polarization and ISHE in a Pt bar thus defines an original nonlocal spin-injection/detection scheme without the use of any ferromagnetic metal, which represents a new paradigm in the field of semiconductor spintronics. To further corroborate this conclusion, the dependence of the ISHE signal ΔV_{ISHE} was measured across the detection Pt stripe as a function of the circular polarization degree and power of the incoming light. The degree of circular polarization has been varied by tuning the phase shift between the two components of the electric field of the light introduced by the photoelastic modulator [see Fig. 2(b)]. Figure 4 reports the dependence of the normalized amplitude A in the function $\Delta V_{\mathrm{ISHE}}/W = Ae^{-x/l_{sf}} \sin(2\pi x/L)$ that better fits the profiles collected along the x axis of the device (see Fig. 3) as a function of the polarization rate and of the impinging power W. In the fitting function, $x = 0$ corresponds to the position of the detector, while $L = 2\ \mu$m stands for the periodicity of the array of the Pt pads, and l_{sf} denotes the spin diffusion length. The ISHE signal is proportional to the degree of circular polarization, hence to the photogenerated polarized spins in the material, while ΔV_{ISHE} tends to saturate at high illumination powers, as expected when a spin current is modulated by the photovoltage across a metal/semiconductor Schottky contact [14,30]. No sizable dependence of the spin diffusion length on the illumination power is observed when the illumination power is within the linearity range of the spin detector, as expected in a linear spin diffusion regime characterized by no interactions between spin carriers.

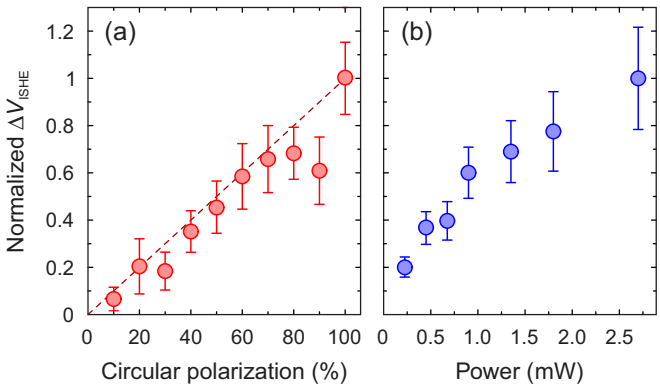

FIG. 4. Dependence of the normalized ΔV_{ISHE} signal on the degree of circular polarization (a) and power (b) of the incident light. ΔV_{ISHE} is obtained from the amplitude coefficient A of the fitting shown in Fig. 3(f), and it has been normalized to unity for a 100% circularly polarized beam with a power equal to 2.9 mW.

IV. CONCLUSIONS

In summary, we have demonstrated pure spin transport in Ge at room temperature using nonlocal optical spin orientation/electrical detection. We used either an MTJ or the ISHE in a Pt stripe to detect the in-plane spin signal generated in the Ge substrate by optical spin orientation at the edge of Pt microstructures. The nonlocal evaluation of the spin accumulation as a function of the location where spin-polarized electrons are generated allows us to map spin diffusion paths inside the Ge substrate and to evaluate the characteristic diffusion lengths. The combination of locally excited optical spin orientation with nonlocal ISHE-based spin detection represents a spintronic platform that is completely free from ferromagnetic functional units and from charge transport.

ACKNOWLEDGMENTS

Financial support from the French National Research Agency through the ANR project SiGeSPIN No. ANR-13-BS10-0002 and from the CARIPLO project SEARCH-IV (Grant No. 2013-0623) is acknowledged. The authors warmly acknowledge Paolo Biagioni for helpful discussion and Laurent Vila for assistance in the fabrication of the microdevices.

[1] D. D. Awschalom and M. E. Flatté, Nat. Phys. **3**, 153 (2007).
[2] I. Žutić, J. Fabian, and S. Das Sarma, Rev. Mod. Phys. **76**, 323 (2004).
[3] S. A. Wolf, D. D. Awschalom, R. A. Buhrman, J. M. Daughton, S. von Molnár, M. L. Roukes, A. Y. Chtchelkanova, and D. M. Treger, Science **294**, 1488 (2001).
[4] P. Li, Y. Song, and H. Dery, Phys. Rev. B **86**, 085202 (2012).
[5] F. Bottegoni, G. Isella, S. Cecchi, and F. Ciccacci, Appl. Phys. Lett. **98**, 242107 (2011).
[6] F. Pezzoli, F. Bottegoni, D. Trivedi, F. Ciccacci, A. Giorgioni, P. Li, S. Cecchi, E. Grilli, Y. Song, M. Guzzi, H. Dery, and G. Isella, Phys. Rev. Lett. **108**, 156603 (2012).
[7] A. Ferrari, F. Bottegoni, G. Isella, S. Cecchi, and F. Ciccacci, Phys. Rev. B **88**, 115209 (2013).
[8] *Optical Orientation*, edited by F. Meier and B. P. Zakharchenya (North-Holland, Amsterdam, 1984).
[9] E. J. Loren, J. Rioux, C. Lange, J. E. Sipe, H. M. van Driel, and A. L. Smirl, Phys. Rev. B **84**, 214307 (2011).
[10] C. Guite and V. Venkataraman, Phys. Rev. Lett. **107**, 166603 (2011).
[11] A. Giorgioni, E. Vitiello, E. Grilli, M. Guzzi, and F. Pezzoli, Appl. Phys. Lett. **105**, 152404 (2014).
[12] C. Rinaldi, M. Cantoni, D. Petti, A. Sottocorno, M. Leone, N. M. Caffrey, S. Sanvito, and R. Bertacco, Adv. Mater. **24**, 3037 (2012).

[13] F. Bottegoni, A. Ferrari, S. Cecchi, M. Finazzi, F. Ciccacci, and G. Isella, Appl. Phys. Lett. **102**, 152411 (2013).
[14] F. Bottegoni, A. Ferrari, F. Rortais, C. Vergnaud, A. Marty, G. Isella, M. Finazzi, M. Jamet, and F. Ciccacci, Phys. Rev. B **92**, 214403 (2015).
[15] F. Bottegoni, C. Zucchetti, S. Dal Conte, J. Frigerio, E. Carpene, C. Vergnaud, M. Jamet, G. Isella, F. Ciccacci, G. Cerullo, and M. Finazzi, Phys. Rev. Lett. **118**, 167402 (2017).
[16] Y. Zhou, W. Han, L.-T. Chang, F. Xiu, M. Wang, M. Oehme, I. A. Fischer, J. Schulze, R. K. Kawakami, and K. L. Wang, Phys. Rev. B **84**, 125323 (2011).
[17] L.-T. Chang, W. Han, Y. Zhou, J. Tang, I. A. Fischer, M. Oehme, J. Schulze, R. K. Kawakami, and K. L. Wang, Semicond. Sci. Technol. **28**, 015018 (2013).
[18] E.-S. Liu, J. Nah, K. M. Varahramyan, and E. Tutuc, Nano Lett. **10**, 3297 (2010).
[19] P. Li, J. Li, L. Qing, H. Dery, and I. Appelbaum, Phys. Rev. Lett. **111**, 257204 (2013).
[20] A. Jain, L. Louahadj, J. Peiro, J. C. L. Breton, C. Vergnaud, A. Barski, C. Beigné, L. Notin, A. Marty, V. Baltz, S. Auffret, E. Augendre, H. Jaffrès, J. M. George, and M. Jamet, Appl. Phys. Lett. **99**, 162102 (2011).
[21] H. Saito, S. Watanabe, Y. Mineno, S. Sharma, R. Jansen, S. Yuasa, and K. Ando, Solid State Commun. **151**, 1159 (2011).
[22] F. Rortais, S. Oyarzún, F. Bottegoni, J.-C. Rojas-Sánchez, P. Laczkowski, A. Ferrari, C. Vergnaud, C. Ducruet, C. Beigné, N. Reyren, A. Marty, J.-P. Attané, L. Vila, S. Gambarelli, J. Widiez, F. Ciccacci, H. Jaffrès, J.-M. George, and M. Jamet, J. Phys.: Condens. Matter **28**, 165801 (2016).
[23] A. Jain, J.-C. Rojas-Sanchez, M. Cubukcu, J. Peiro, J. C. Le Breton, E. Prestat, C. Vergnaud, L. Louahadj, C. Portemont, C. Ducruet, V. Baltz, A. Barski, P. Bayle-Guillemaud, L. Vila, J.-P. Attané, E. Augendre, G. Desfonds, S. Gambarelli, H. Jaffrès, J.-M. George, and M. Jamet, Phys. Rev. Lett. **109**, 106603 (2012).
[24] A. Jain, C. Vergnaud, J. Peiro, J. C. L. Breton, E. Prestat, L. Louahadj, C. Portemont, C. Ducruet, V. Baltz, A. Marty, A. Barski, P. Bayle-Guillemaud, L. Vila, J.-P. Attané, E. Augendre, H. Jaffrès, J.-M. George, and M. Jamet, Appl. Phys. Lett. **101**, 022402 (2012).
[25] K.-R. Jeon, B.-C. Min, Y.-H. Jo, H.-S. Lee, I.-J. Shin, C.-Y. Park, S.-Y. Park, and S.-C. Shin, Phys. Rev. B **84**, 165315 (2011).
[26] A. Hanbicki, S.-F. Cheng, R. Goswami, O. van't Erve, and B. Jonker, Solid State Commun. **152**, 244 (2012).
[27] S. Iba, H. Saito, A. Spiesser, S. Watanabe, R. Jansen, S. Yuasa, and K. Ando, Appl. Phys. Express **5**, 053004 (2012).
[28] S. Dushenko, M. Koike, Y. Ando, T. Shinjo, M. Myronov, and M. Shiraishi, Phys. Rev. Lett. **114**, 196602 (2015).
[29] G. Isella, F. Bottegoni, A. Ferrari, M. Finazzi, and F. Ciccacci, Appl. Phys. Lett. **106**, 232402 (2015).
[30] F. Bottegoni, C. Zucchetti, F. Ciccacci, M. Finazzi, and G. Isella, Appl. Phys. Lett. **110**, 042403 (2017).
[31] J. Rioux and J. E. Sipe, Phys. Rev. B **81**, 155215 (2010).
[32] F. Bottegoni, M. Celebrano, M. Bollani, P. Biagioni, G. Isella, F. Ciccacci, and M. Finazzi, Nat. Mater. **13**, 790 (2014).
[33] K. Kasahara, Y. Fujita, S. Yamada, K. Sawano, M. Miyao, and K. Hamaya, Appl. Phys. Express **7**, 033002 (2014).
[34] C. Rinaldi, S. Bertoli, M. Asa, L. Baldrati, C. Manzoni, M. Marangoni, G. Cerullo, M. Bianchi, R. Sordan, R. Bertacco, and M. Cantoni, J. Phys. D **49**, 425104 (2016).
[35] A. L. Smirl, S. C. Moss, and J. R. Lindle, Phys. Rev. B **25**, 2645 (1982).
[36] T. Yu and M. W. Wu, J. Phys.: Condens. Matter **27**, 255001 (2015).